Removing or Truncating Connexin 43 in Murine Osteocytes Alters Cortical Geometry, Nanoscale Morphology, and Tissue Mechanics in the Tibia

Max A. Hammond[a], **Alycia G. Berman**[b], **Rafael Pacheco-Costa**[c], **Hannah M. Davis**[c], **Lilian I. Plotkin**[c,d], and **Joseph M. Wallace**[b,e]

[a]Weldon School of Biomedical Engineering, Purdue University, West Lafayette, IN

[b]Department of Biomedical Engineering, Indiana University-Purdue University at Indianapolis, IN

[c]Department of Anatomy and Cell Biology, Indiana University School of Medicine, IN

[d]Roudebush Veterans Administration Medical Center, Indianapolis, IN

[e]Department of Orthopaedic Surgery, Indiana University School of Medicine, IN

Abstract

Gap junctions are formed from ubiquitously expressed proteins called connexins that allow the transfer of small signaling molecules between adjacent cells. Gap junctions are especially important for signaling between osteocytes and other bone cell types. The most abundant type of connexin in bone is connexin 43 (Cx43). The C-terminal domain of Cx43 is thought to be an important modulator of gap junction function but the role that this domain plays in regulating tissue-level mechanics is largely unknown. We hypothesized that the lack of the C-terminal domain of Cx43 would cause morphological and compositional changes as well as differences in how bone responds to reference point indentation (RPI) and fracture toughness testing. The effects of the C-terminal domain of Cx43 in osteocytes and other cell types were assessed in a murine model (C57BL/6 background). Mice with endogenous Cx43 in their osteocytes removed via a Cre-loxP system were crossed with knock-in mice which expressed Cx43 that lacked the C-terminal domain in all cell types due to the insertion of a truncated allele to produce the four groups used in the study. The main effect of removing the C-terminal domain from osteocytic Cx43 increased cortical mineral crystallinity (p=0.036) and decreased fracture toughness (p=0.017). The main effect of the presence of the C-terminal domain in other cell types increased trabecular thickness (p<0.001), cortical thickness (p=0.008), and average RPI unloading slope (p=0.004). Collagen morphology was altered when either osteocytes lacked Cx43 (p=0.008) or some truncated Cx43 was expressed in all cell types (p<0.001) compared to controls but not when only the truncated form of Cx43 was expressed in osteocytes (p=0.641). In conclusion, the presence of the C-terminal

Corresponding Author: Dr. Joseph M. Wallace, Indiana University-Purdue University at Indianapolis, Department of Biomedical Engineering, 723 W Michigan St. SL220D, Indianapolis, IN 46202, Phone: (317) 274-2448, Fax: (317) 278-2455, jmwalla@iupui.edu.

domain of Cx43 in osteocytes and other cell types is important to maintain normal structure and mechanical integrity of bone.

Keywords

type I collagen; reference point indentation; Raman spectroscopy; atomic force microscopy; fracture toughness; bone

1. INTRODUCTION

Gap junctions are ubiquitously expressed protein channels that allow for rapid signaling between adjacent cells by linking the cells' cytoplasm and permitting ions and small molecules (< 1 kDa) to be transported between the cells.[1] The most common gap junction channel in bone is formed from connexin 43 (Cx43) wherein six Cx43 molecules assemble into a hemichannel in each cell and the two hemichannels dock to complete the gap junction.[2] In bone gap junctions are important for communication within the osteocyte network and between osteocytes and other cell types on the surface of bone to coordinate structural changes and respond to mechanical loading/unloading.[3–6] The clinical importance of proper Cx43 gap junctions function is apparent in oculodentoligcal dysplasia (ODDD) which is characterized by craniofacial and skeletal abnormalities caused by mutations in *GJA1* that result in amino acid changes at critical highly conserved locations in Cx43's structure.[7]

Cx43's structure consists of an intracellular amino terminus, four transmembrane loops connected by two extracellular loops and one intracellular loop, and an intracellular carboxyl terminus.[1] The N-terminal domain is small compared to the C-terminal domain and modulates the voltage-gated behavior of the channel whereas the larger C-terminal domain serves as a scaffold for downstream signaling molecules to associate with the channel and regulates channel closing.[8–10] Due to both channel dependent and independent functions of the C-terminal domain,[11, 12] it has been the target of recent research. However, the role the C-terminal domain plays in regulating the quality and mechanical integrity of bone tissue is a largely uninvestigated area despite evidence that tissue-level mechanical properties are altered at the macroscale with the removal of Cx43.[13, 14] Additionally, while studies have investigated conditional knock outs of Cx43 in either osteoblasts and osteocytes or only osteocytes,[4, 6, 14] the role the C-terminal domain plays in determining tissue quality was not directly investigated and was limited to its modulation of parathyroid hormone treatment.[13]

The current study sought to address the importance of the C-terminal domain of Cx43 within osteocytes and other cell types in determining the microscale mechanics of bone by identifying changes in tissue composition that could alter the bone's mechanical integrity, e.g. collagen morphology. To assess the role of C-terminal domain, genetically modified mice were used that either express a truncated form of Cx43 without the C-terminal domain or lack endogenous Cx43 in their osteocytes.[6, 15] Changes to the nanoscale morphology of collagen due to the altered Cx43-mediated signaling were investigated for the first time. We hypothesized that the lack of the C-terminal domain of Cx43 would alter collagen

morphology, tissue composition, and mechanical properties as measured by reference point indentation and fracture toughness testing in a murine model.

2. MATERIALS AND METHODS

2.1 Animals

Knock-in mice containing one allele coding for endogenous Cx43 and a mutant allele that has the C-terminal end of the Cx43 truncated at amino acid 258 (Cx43K258stop)[15] were crossed with mice having two loxP-flanked (floxed) endogenous Cx43 encoding alleles (fl/fl)[16] to generate mice with one truncated Cx43 allele and one floxed allele (ΔCT/fl). ΔCT/fl mice were bred with mice expressing Cre recombinase under the control of an 8kb fragment of murine dentin matrix protein 1 promoter (DMP1-8kb-Cre) with both alleles floxed (fl/fl:Cre) which selectively removes Cx43 from osteocytes.[6] This cross resulted in mice able to express endogenous Cx43 in all cell types (fl/fl), mice lacking Cx43 in osteocytes but able to express endogenous Cx43 in all other cell types (fl/fl:Cre), mice able to express both endogenous and truncated Cx43 in all cell types (ΔCT/fl), and mice able to express only truncated Cx43 in their osteocytes but able to express both endogenous and truncated Cx43 in all other cell types (ΔCT/fl:Cre). All mice were developed on a C57BL/6 background, given *ad libitum* access to food and water, and kept in a 12 hour light/dark cycle environment. After sacrifice via cervical dislocation while under isoflurane anesthesia, left and right tibiae were harvested from four month old female mice, cleaned of soft tissue, snap frozen in liquid nitrogen, and stored at −80 °C. All work was performed with prior IACUC approval from the Indiana University School of Medicine.

2.2 Raman Spectroscopy

Samples were submerged in a PBS bath and allowed to thaw for 30 minutes. Once thawed, the periosteum was stripped from the medial surface of the right tibiae and PBS was removed from the bath until only the medial surface was exposed (n=6–12 per group). A LabRAM HR 800 Raman Spectrometer (HORIBA Jobin Yvon, Edison, NJ) with a 660 nm laser focused on the exposed surface (spot size of ~10 μm) through an integrated BX41 microscope (Olympus, Tokyo, Japan) with a 50× objective (NA=0.75) was used to record Raman spectra. Five locations were measured between the medial malleolus and the tibia-fibula junction (TFJ) 1–2 mm apart along the native medial surface of the bone while in the PBS bath. Five 20 second acquisitions were averaged at each location between 700 cm^{-1} and 1800 cm^{-1} and a 5 point linear baseline correction was applied in LabSpec 5 (HORIBA Jobin Yvon). The areas of the PO_4^{3-} ν1, CO_3^{2-} ν1, and Amide III bands and the full width at half maximum (FWHM) of a Gaussian fit of the PO_4^{3-} ν1 peak were calculated using OriginPro 8.6 (OriginLab, Northampton, MA) at each location as previously described.[17] Type B carbonate substitution, crystallinity/maturity, and relative matrix mineralization were defined as the band area ratio of CO_3^{2-} ν1/ PO_4^{3-} ν1, 1/FWHM of PO_4^{3-} ν1, and band area ratio of PO_4^{3-} ν1 /Amide III, respectively. Following imaging, samples were wrapped in PBS soaked gauze and stored at −20 °C.

2.3 Reference Point Indentation (RPI)

RPI was performed using a BioDent Hfc microindenter (Active Life Scientific, Santa Barbara, CA) in the same region and along the same surface as Raman spectroscopy locations on the right tibiae (n=6–12 per group). Beginning just proximal to the medial malleolus, 4–5 locations 1–1.5 mm apart were indented using Bone Probe 3 (BP3) along the medial surface of the bone while submerged in a PBS bath and secured in the manufacturer provided stage. Ten cycles of a 2 N indentation force were applied at a frequency of 2 Hz. A custom MATLAB (MathWorks, Natick, Massachusetts) program was used to calculate the 1st cycle indentation distance (ID 1st), 1st cycle energy dissipation (ED 1st), 1st cycle unloading slope (US 1st), 1st cycle creep indentation distance (CID 1st), indentation distance increase (IDI), total indentation distance (TID), total energy dissipation (ED Tot), average creep indentation distance (CID Avg), average energy dissipation from cycles 3–10 (ED Avg), and average unloading slope (US Avg).[18] Following imaging, samples were wrapped in PBS soaked gauze and stored at −20 °C.

2.4 Atomic Force Microscopy

After Raman and RPI, a 6 mm section between the TFJ and malleoli was removed using a low speed sectioning saw, mounted lateral-side up to a steel disk with cyanoacrylate glue, and polished using a 3 μm diamond suspension (n=4 per group). Each sample was treated for 15 minutes with 0.5 M EDTA at a pH of 8.0 followed by sonication for 5 minutes in ultrapure water. This process was repeated 3 times. Samples were imaged using a BioScope Catalyst AFM in peak force tapping mode (Bruker, Santa Barbara, CA). A 3.5 μm × 3.5 μm image was acquired from 4–5 locations spaced ~1 mm apart along the polished surface of the sample using a silicon cantilever with a silicon probe (tip radius ~ 8 nm). From each error image, 2D Fast Fourier Transforms (2D FFTs) were performed on 10–15 fibrils (50–60 fibrils per bone) to obtain an individual fibril's D-spacing from the first harmonic peak of the power spectrum as previously described.[17, 19, 20]

2.5 Micro-computed Tomography (μCT)

Left tibiae were thawed and hydrated for 30 minutes in PBS. Samples were wrapped in Parafilm M (Bemis, Oshkosh, WI) to maintain hydration and were scanned in air with the long axis of the bone vertical using a Skyscan 1172 system (Bruker microCT, Kontich, Belgium; n=6–9 per group). Scans were performed using a 12.5 μm voxel size with a source voltage of 59 kV and current of 167 μA through a 0.5 mm Al filter. NRecon (Bruker microCT) was used to reconstruct voxels with attenuation coefficients ranging from 0–0.11, apply a beam hardening correction of 40%, and apply a ring artifact correction of 5. Mineral density was calculated using daily scans of manufacturer supplied hydroxyapatite (HA) phantoms of 0.25 g/cm^3 and 0.75 g/cm^3. Reconstructed scans were rotated using Dataviewer (Bruker microCT) to ensure precise vertical alignment. The metaphyseal region of interest extended from the distal end of the proximal growth plate to 10% of the distance between the growth plate and the TFJ. A custom MATLAB script segmented the cortical shell from trabecular region of interest which followed the contour of the cortical shell in each slice. CTAn (Bruker microCT) was used to compute bone volume fraction (BV/TV), trabecular thickness (Tb.Th), trabecular separation (Tb.Sp), trabecular number (Tb.N), structure model

index (SMI), connectivity density (Conn.Dn), and bone mineral density (BMD). The cortical standard site was defined as a 7 slice region centered on the slice that was 80% the distance between the growth plate and the TFJ from the growth plate. A custom MATLAB script was used to calculate total bone area (B.Ar), marrow area (Ma.Ar), cortical area (Ct.Ar), cortical width (Ct.Wi), periosteal perimeter (Ps.Pm), endocortical perimeter (Ec.Pm), maximum second moment of inertia (I_{max}), minimum second moment of inertia (I_{min}), and tissue mineral density (TMD). Following imaging, samples were wrapped in PBS soaked gauze and stored at −20 °C.

2.6 Fracture Toughness

A notch was cut into the medullary cavity through the anteromedial side of the left tibia approximately 1.75 mm above the TFJ by hand using a scalpel blade lubricated with a 1 μm diamond suspension to a depth not exceeding the midpoint of the bone (n=6–9 per group). The samples were tested to failure in three-point bending at a rate of 0.001 mm/sec with the notch in tension and directly under the applied load. The location of the fracture site was measured with calipers and the geometric properties of the fracture site were determined using μCT. After dehydration with graded ethanol (70–100%), samples were mounted to a stainless steel stub using carbon tape, gold-coated, and the fracture surface imaged using SEM to obtain the angles of stable and unstable crack growth. The force and displacement data, geometric properties, and crack growth angles were used to calculate fracture stress intensity factor (K_c) using a custom MATLAB script.[21, 22]

2.7 Statistical Analysis

Multiple locations within the same sample (Raman, RPI, and AFM) were averaged to yield a single sample value for mean comparisons between groups. A two-way ANOVA testing the main effects of the fl:Cre and CT alleles as well as their interaction was applied to examine mean differences. Only when an interaction between main effects was likely (p<0.10) was a one-way ANOVA applied to reveal pairwise differences between groups with a post hoc Tukey test. For the main effects and pairwise comparisons, p<0.05 was considered significant. Unless explicitly stated, all p-values reported are two-way ANOVA p-values from the main effects of the fl:Cre and CT. Because both main effects had only two levels, additional post hoc tests were not necessary in the presence of a significant main effect without an interaction. Applying an additional statistical model to the same data (e.g. a one-way ANOVA to perform pairwise comparisons between groups) without the presence of an interaction would not be valid. A custom written MATLAB script was used to verify the assumptions of normality and homoscedasticity, transform the data if necessary, and run the ANOVA for each variable. To test if D-spacing distributions were significantly different, a k-sample Anderson-Darling (AD) test was used and post hoc pairwise AD tests with a Bonferroni correction (α' = 0.05 / 6) were used to test for differences between individual groups. All data are presented as mean ± SD. For all assays, a single technician performed the imaging and analysis in random order while blinded.

3. RESULTS

3.1 Animals

No adverse events were noted at any time for any animal in the study. The average weight for all mice was 21.5 ± 3.28 g and was not different between groups. Unequal sample sizes between groups were solely due to the results of the cross and no animal was excluded from the study.

3.2 Raman spectroscopy

Crystallinity was significantly increased by removing endogenous Cx43 from osteocytes (main effect of fl:Cre p=0.036; Table 1). Type B carbonate substitution and relative matrix mineralization were statistically indistinguishable between groups as shown in Table 1. There were no significant interactions for any Raman parameters.

3.3 Reference Point Indentation

The presence of truncated Cx43 significantly decreased the 1st cycle and average unloading slopes (p=0.008 and p=0.004, respectively; Table 2). The removal of endogenous Cx43 resulted in a decreasing trend for both 1st cycle and average unloading slope, but failed to reach significance (p=0.058 and p=0.062, respectively). Removing endogenous Cx43 significantly increased the average energy dissipation (p=0.027). No interactions were present for any RPI parameters.

3.4 Atomic Force Microscopy

The mean collagen D-spacing for each group was 64.7 ± 1.2 nm, 65.5 ± 1.4 nm, 66.0 ± 1.2 nm, and 64.8 ± 1.1 nm for fl/fl, fl/fl:Cre, CT/fl, and CT/fl:Cre, respectively. No significant changes in mean collagen D-spacing were observed due to the main effects of fl:Cre, CT, or their interaction. In the fl/fl:Cre group, the absence of Cx43 in osteocytes resulted in a significantly different collagen D-spacing distribution compared to the fl/fl control group (p=0.0079; fl/fl n = 219 fibrils; fl/fl:Cre n = 228 fibrils) which was shifted to higher D-spacing values (Figure 1A). In the CT/fl group, the addition of truncated Cx43 also resulted in a significantly different D-spacing distribution that was shifted to higher values compared to the fl/fl control (p<0.0001; CT/fl n= 226 fibrils; Figure 1B). The distributions of fl/fl:Cre and CT/fl were not statistically different (p=0.1819). For CT/fl:Cre when endogenous Cx43 was removed from osteocytes in the presence of the truncated Cx43, the D-spacing distribution was significantly different than that of the CT/fl group (p=0.0002; CT/fl:Cre n = 221 fibrils), but the distribution was shifted to lower values as opposed to the upward shift noted between the fl/fl and fl/fl:Cre groups in Figure 1A. While the direction was reversed, the magnitude of the shift was approximately equal so that the D-spacing distribution of the CT/fl:Cre group was statistically indistinguishable from the fl/fl group (p=0.6407; Figure 1C). Despite a p-value less than 0.05, the distribution of CT/fl:Cre was statistically indistinguishable from fl/fl:Cre given the Bonferroni correction (p=0.0428).

3.5 Trabecular Analysis

Microarchitectural changes in the proximal metaphysis of the tibia were dominated by the addition of truncated Cx43 rather than the removal of endogenous Cx43 from osteocytes with Cre recombinase. There were no significant effects due to main effect of fl:Cre. As seen in Table 3, the addition of truncated Cx43 caused thicker (p<0.001) and more rod-like trabecular struts to develop (p=0.001). However, the number of trabeculae present was reduced (p=0.047) resulting in a less connected microarchitecture (p=0.044) and a non-significant trend for increased trabecular separation (p=0.080). The reduction in trabecular number dominated the effects of increased trabecular thickness which caused a significant decrease in BMD (p=0.029) although bone volume fraction was statistically indistinguishable. There were no significant interactions between fl:Cre and ΔCT for any of these parameters.

3.6 Cortical Analysis

Normality could not be restored with data transformations for endocortical perimeter or marrow area. Therefore, the statistical analyses for these two parameters were performed on ranked data. As seen in Table 4, removing endogenous Cx43 from osteocytes (main effect of fl:Cre) increased total bone area (p=0.005), marrow area (p<0.001), endocortical perimeter (p<0.001), and minimum second moment of inertia (p=0.025). Expressing truncated Cx43 (main effect of ΔCT) had the opposite effect and reduced the total bone area (p=0.001), marrow area (p=0.011), endocortical perimeter (p=0.031), and minimum second moment of inertia (p=0.030). However, the width of the cortical shell was increased due to an endocortical contraction primarily along the mediolateral axis (Figure 2B and Figure 2C) when truncated Cx43 was present (p=0.008). The main effects of fl:Cre and ΔCT had a significant interaction for periosteal perimeter (p=0.006) and tissue mineral density (p=0.024). An underlying interaction also was suspected for maximum second moment of inertia (p=0.087) and these three parameters were analyzed using a one-way ANOVA. Post hoc analyses from the one-way ANOVA revealed that the interactive effect in these three parameters was primary driven by the fl/fl:Cre group (Table 4). The differences between the fl/fl:Cre group and the other groups were due to a large periosteal expansion in the posterior direction (Figure 2A) that was corrected with the addition of the truncated Cx43 (Figure 2D).

3.7 Fracture Toughness

Two samples from the fl/fl:Cre group and one sample from the ΔCT/fl:Cre group were damaged during notching and were excluded. The removal of endogenous Cx43 from osteocytes decreased the ability of the tissue to resist crack propagation as demonstrated by the significant reductions in K_c (Figure 3) for crack initiation (p=0.030), maximum load (p=0.032), and fracture instability methods (p=0.017). No effects were observed due to the main effect of ΔCT, and there were no significant interactions.

4. DISCUSSION

The selective removal of Cx43 from osteocytes alters the morphology of collagen (Figure 1A) which is interesting given that the collagen was presumably previously deposited by

osteoblasts with endogenous Cx43. Removing Cx43 from osteocytes increases osteocyte apoptosis,[6] but it is unclear whether the apoptotic debris (e.g. enzymes and growth factors that could alter the extracellular milieu) or local alteration of the collagen matrix by osteocytes would affect a sufficient volume to result in the change noted here. AFM locations were randomly chosen along the polished length of the bone without regard to the position of osteocyte lacunae and areas both away from and directly adjacent to osteocyte lacunae and/or dendritic processes are expected to be present in the sampling of the collagen matrix. While blocking lysyl oxidase (LOX) function with β-aminopropionitrile alters D-spacing distribution and fl/fl:Cre mice have reduced LOX expression, enzymatic crosslinks are not likely to contribute to the D-spacing shift noted here given the shift is not in the expected direction and crosslink maturity was not significantly affected despite reduced LOX expression.[14, 20]

While the shifts in D-spacing caused by the removal of full-length Cx43 from osteocytes and the shift accompanying the truncation of the C-terminal domain of Cx43 in all cell types are similar (Figure 1), it is important to note that there is an interactive effect at play when both endogenous Cx43 is removed from osteocytes and the truncated Cx43 is expressed. Two separate mechanisms may be present when Cx43 is removed from osteocytes and when Cx43 is truncated. The distribution shift observed between fl/fl and ΔCT/fl may be driven by the presence of the truncated form of Cx43 in osteoblasts which is mitigated by either the complete removal of the C-terminus of Cx43 from osteocytes or a possible reduction in Cx43 expression in ΔCT/fl:Cre. Another possibility may be that the heterogeneity of the gap junctions when both endogenous and truncated Cx43 was present resulted in the interactive effect observed for the D-spacing as uniform distribution of Cx43 in osteocytes would be restored in ΔCT/fl:Cre mice. However, future research is needed to test these hypotheses and account for the interactive effect on D-spacing.

The pattern of differences noted in D-spacing distribution was not observed for any other parameters, but there were interactions in cortical geometry that were driven by alterations in the fl/fl:Cre group that were not present in other groups (Table 4). The expanded cortical geometry in fl/fl:Cre (Figure 2A) was similar to previous reports and not present in other groups (Figure 2B–D).[4, 6] While this expansion altered the distribution of material in the bone and would increase the section modulus, the deficient mineral density in fl/fl:Cre would likely negate any beneficial effect. The difference between fl/fl:Cre and all other groups was the lack of the transmembrane domains, their connecting loops, and N-terminal domains of Cx43 in the osteocytes of these mice. Therefore, one can conclude that the presence of these domains and not the C-terminal domain in osteocytes is integral to the regulation of cortical geometry by Cx43 as suggested by the lack of ODDD-inducing mutations in the C-terminal domain.[8]

While the C-terminal domain may not be vital for periosteal expansion, the presence of this domain in osteocytes is crucial to preserve tissue level mechanical integrity. When osteocytes are not able to express any Cx43 containing the C-terminal domain (fl/fl:Cre and ΔCT/fl:Cre), bone's ability to resist crack propagation was decreased (as demonstrated by the decreased fracture toughness measures in Figure 3). This effect also was observed at the microscale as increased average energy dissipation (Table 2) likely due to damage induced

during the first indentation cycle propagating through the bone easier during subsequent cycles thereby dissipating more energy. Increased mineral crystallinity with the absence of the Cx43 C-terminus in osteocytes may explain the tissue's increased proclivity to crack propagation. Larger crystallites are suspected of decreasing the deformability of bone and post-yield properties,[23] which could decrease toughness and allow greater crack propagation. A previous study using Fourier Transform Infrared Imaging (FTIRI) did not observe differences in crystallinity in the femoral diaphysis between fl/fl and fl/fl:Cre mice although there was a slight non-significant increase.[14] The differences between these observations and the data presented here may be due to the differences in method (FTIRI vs Raman spectroscopy), sample preparation (5 μm sections of embedded bone vs native hydrated surface), sample location (femur vs tibia), or statistical design (Mann–Whitney U test with 6 total samples vs two-way ANOVA with 34 total samples).

The presence of the C-terminal domain of Cx43 is also important for cell types other than osteocytes and reducing the amount of Cx43 molecules containing this domain in other cells (e.g. osteoblasts) results in altered cortical geometry, trabecular architecture, and microscale mechanics (main effect of CT). The increased average and first unloading slopes suggests that the bone is stiffer on a microscale which may be due to increased TMD. While the interactive effect for TMD prevented statistically testing the main effect of CT, TMD is modestly elevated in the CT/fl and CT/fl:Cre groups compared to fl/fl (Table 3). In regard to only the C-terminal domain, the main effect of CT was the result of removing it from only one allele whereas the main effect of fl:Cre was the result of removing the C-terminal domain from both alleles in osteocytes (by way of completely removing Cx43 due to Cre). There were no interactions due to CT/fl despite that group having only one allele capable of producing the C-terminal domain in its osteocytes. The CT/fl group did not result in an intermediate phenotype when there was a main effect of fl:Cre indicating that only some osteocytic Cx43 containing the C-terminal domain is necessary for proper function. Therefore, osteocytes are not as sensitive as other cell types to the presence of the C-terminal domain of Cx43.

While this study was able to highlight the effects of the C-terminal domain of Cx43 in osteocytes and other cell types, the study was not without its limitations. Removing floxed Cx43 with Cre allowed us to investigate the absence of the C-terminal domain in osteocytes but the effects are confounded by the complete removal of Cx43 in the fl/fl:Cre group. Additionally, it is unclear if the effects noted in CT/fl:Cre may be partially due to a reduction in the total amount of Cx43 present in osteocytes as it is not known if the expression of the truncated form of Cx43 is increased to compensate for the loss of one allele. The expression of both the endogenous and truncated forms of Cx43 may result in a distribution of phenotypes given the dodecameric nature of gap junctions and the many combinations of truncated and endogenous Cx43 that could be present in any given gap junction. While changes are discussed in relation to intercellular signaling via gap junctions, undocked hemichannels allow the exchange of ions and small molecules between the cytoplasm and the extracellular milieu,[24] and these changes to the extracellular environment may influence the effects noted here.

5. CONCLUSIONS

The presence of the C-terminal domain of Cx43 was important to maintain normal structure and mechanical integrity of bone. However, the presence of the other domains of Cx43 was necessary to maintain proper tissue mineral density. Removing the C-terminal domain from osteocytes reduced fracture toughness and increased bone area whereas removing this domain from other cell types resulted in bone that was more resistant to microscale indentation with thicker trabeculae and a thicker cortical shell. Future research should be aimed at determining the toughening mechanisms attributed to the C-terminal domain of Cx43 in osteocytes and isolating the role of this domain independent of reducing the amount of Cx43 expressed. Altering Cx43 specifically in osteocytes shifted the D-spacing distribution of collagen and future research into the feedback mechanism between gap junction-mediated cell signaling in osteocytes and collagen morphology is needed.

Acknowledgments

REFERENCES

1. Goodenough DA, Paul DL. Gap junctions. Cold Spring Harb Perspect Biol. 2009; 1(1):a002576. [PubMed: 20066080]

2. Plotkin LI, Stains JP. Connexins and pannexins in the skeleton: gap junctions, hemichannels and more. Cell Mol Life Sci. 2015; 72(15):2853–2867. [PubMed: 26091748]

3. Yellowley CE, Li Z, Zhou Z, Jacobs CR, Donahue HJ. Functional gap junctions between osteocytic and osteoblastic cells. J Bone Miner Res. 2000; 15(2):209–217. [PubMed: 10703922]

4. Bivi N, Pacheco-Costa R, Brun LR, et al. Absence of Cx43 selectively from osteocytes enhances responsiveness to mechanical force in mice. J Orthop Res. 2013; 31(7):1075–1081. [PubMed: 23483620]

5. Lloyd SA, Loiselle AE, Zhang Y, Donahue HJ. Connexin 43 deficiency desensitizes bone to the effects of mechanical unloading through modulation of both arms of bone remodeling. Bone. 2013; 57(1):76–83. [PubMed: 23891909]

6. Bivi N, Condon KW, Allen MR, et al. Cell autonomous requirement of connexin 43 for osteocyte survival: Consequences for endocortical resorption and periosteal bone formation. J Bone Miner Res. 2012; 27(2):374–389. [PubMed: 22028311]

7. Paznekas WA, Boyadjiev SA, Shapiro RE, et al. Connexin 43 (GJA1) mutations cause the pleiotropic phenotype of oculodentodigital dysplasia. The American Journal of Human Genetics. 2003; 72(2):408–418. [PubMed: 12457340]

8. Gemel J, Lin X, Veenstra RD, Beyer EC. N-terminal residues in Cx43 and Cx40 determine physiological properties of gap junction channels, but do not influence heteromeric assembly with each other or with Cx26. J Cell Sci. 2006; 119(11):2258–2268. [PubMed: 16723732]

9. Dbouk HA, Mroue RM, El-Sabban ME, Talhouk RS. Connexins: a myriad of functions extending beyond assembly of gap junction channels. Cell Commun Signal. 2009; 7(4)

10. Giepmans, BNG. Role of Connexin43-Interacting Proteins at Gap Junctions. Cardiovascular Gap Junctions: S. Karger AG; 2006. p. 41-56.

11. Crespin S, Bechberger J, Mesnil M, Naus CC, Sin W-C. The carboxy-terminal tail of connexin43 gap junction protein is sufficient to mediate cytoskeleton changes in human glioma cells. J Cell Biochem. 2010; 110(3):589–597. [PubMed: 20512920]

12. Dang X, Jeyaraman M, Kardami E. Regulation of connexin-43-mediated growth inhibition by a phosphorylatable amino-acid is independent of gap junction-forming ability. Mol Cell Biochem. 2006; 289(1–2):201–207. [PubMed: 16718370]

13. Pacheco-Costa R, Davis HM, Sorenson C, et al. Defective cancellous bone structure and abnormal response to PTH in cortical bone of mice lacking Cx43 cytoplasmic C-terminus domain. Bone. 2015; 81:632–643. [PubMed: 26409319]

14. Bivi N, Nelson MT, Faillace ME, Li J, Miller LM, Plotkin LI. Deletion of Cx43 from osteocytes results in defective bone material properties but does not decrease extrinsic strength in cortical bone. Calcif Tissue Int. 2012; 91(3):215–224. [PubMed: 22865265]

15. Maass K, Ghanem A, Kim J-S, et al. Defective epidermal barrier in neonatal mice lacking the C-terminal region of connexin43. Mol Biol Cell. 2004; 15(10):4597–4608. [PubMed: 15282340]

16. Theis M, de Wit C, Schlaeger TM, et al. Endothelium-specific replacement of the connexin43 coding region by a lacZ reporter gene. Genesis. 2001; 29(1):1–13. [PubMed: 11135457]

17. Hammond MA, Gallant MA, Burr DB, Wallace JM. Nanoscale changes in collagen are reflected in physical and mechanical properties of bone at the microscale in diabetic rats. Bone. 2014; 60(0): 26–32. [PubMed: 24269519]

18. Aref M, Gallant MA, Organ JM, et al. In vivo reference point indentation reveals positive effects of raloxifene on mechanical properties following 6 months of treatment in skeletally mature beagle dogs. Bone. 2013; 56(2):449–453. [PubMed: 23871851]

19. Wallace JM, Chen Q, Fang M, Erickson B, Orr BG, Banaszak Holl MM. Type I collagen exists as a distribution of nanoscale morphologies in teeth, bones, and tendons. Langmuir. 2010; 26(10): 7349–7354. [PubMed: 20121266]

20. Hammond MA, Wallace JM. Exercise prevents [beta]-aminopropionitrile-induced morphological changes to type I collagen in murine bone. BoneKEy Rep. 2015; 4:645. [PubMed: 25798234]

21. Ritchie R, Koester K, Ionova S, Yao W, Lane N, Ager J III. Measurement of the toughness of bone: a tutorial with special reference to small animal studies. Bone. 2008; 43(5):798–812. [PubMed: 18647665]

22. ASTM Standard E399, 2012e3. Standard test method for linear-elastic plane-strain fracture toughness KIC of metallic materials. West Conshohocken, PA: ASTM International; 2012.

23. Yerramshetty JS, Akkus O. The associations between mineral crystallinity and the mechanical properties of human cortical bone. Bone. 2008; 42(3):476–482. [PubMed: 18187375]

24. Goodenough DA, Paul DL. Beyond the gap: functions of unpaired connexon channels. Nature Reviews Molecular Cell Biology. 2003; 4(4):285–295. [PubMed: 12671651]

Highlights

- Murine model with connexin 43 lacking C-terminus or removed from osteocytes used

- Bone quality, mechanics, and morphology assessed in tibiae

- Collagen morphology altered if connexin 43 removed or truncated

- C-terminal domain of connexin 43 in osteocytes maintains fracture toughness

- Global lack of C-terminal domain alters microarchitecture and microscale mechanics
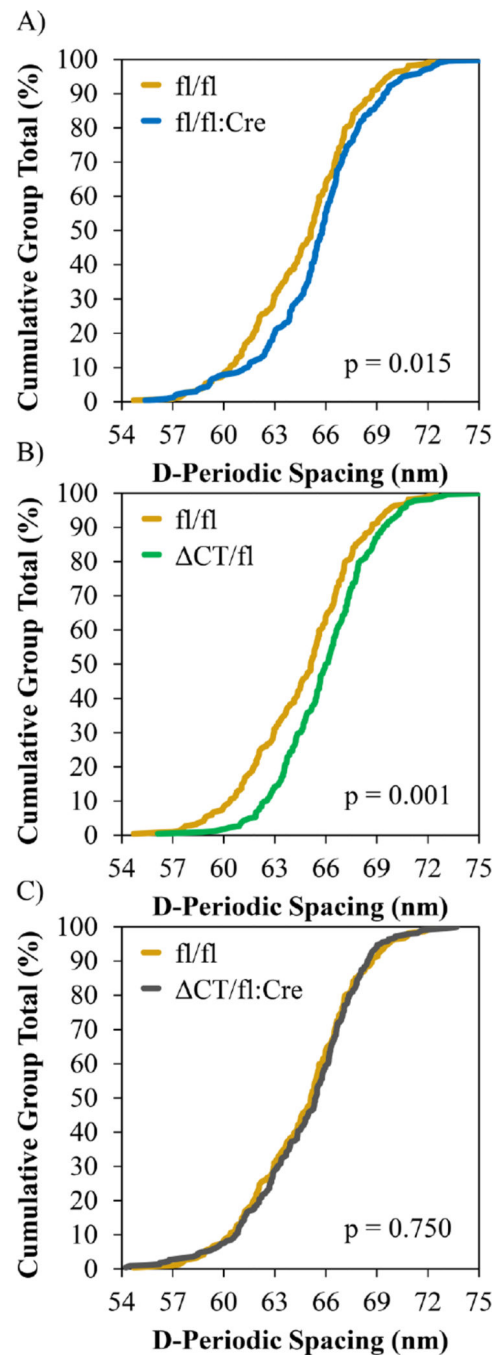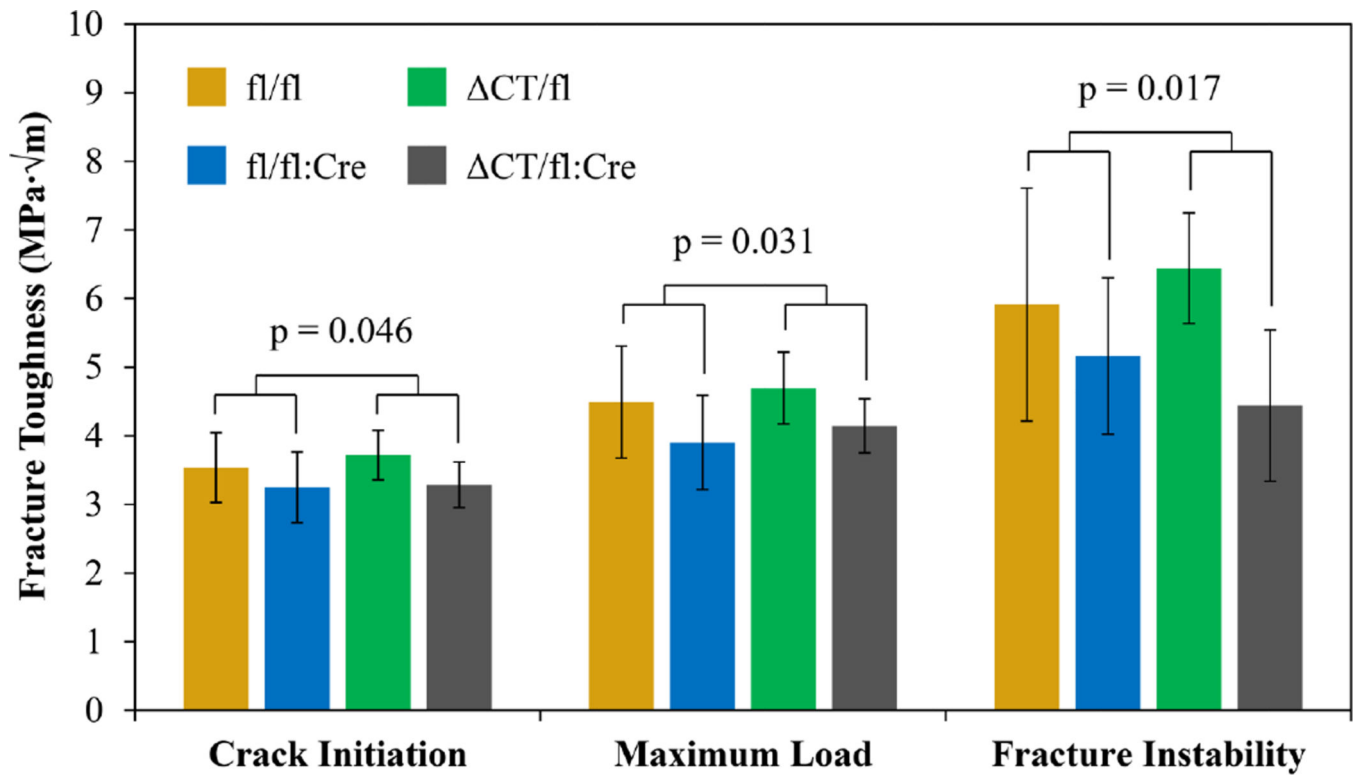
Figure 1.
AFM D-spacing distributions from lateral surface of distal right tibiae. A) Removing Cx43 from osteocytes significantly shifts the D-spacing distribution to higher values. B) Expressing the truncated form of Cx43 also shifts the D-spacing distribution to higher values. C) When only the truncated Cx43 is expressed in osteocytes the distribution is indistinguishable from the fl/fl control.
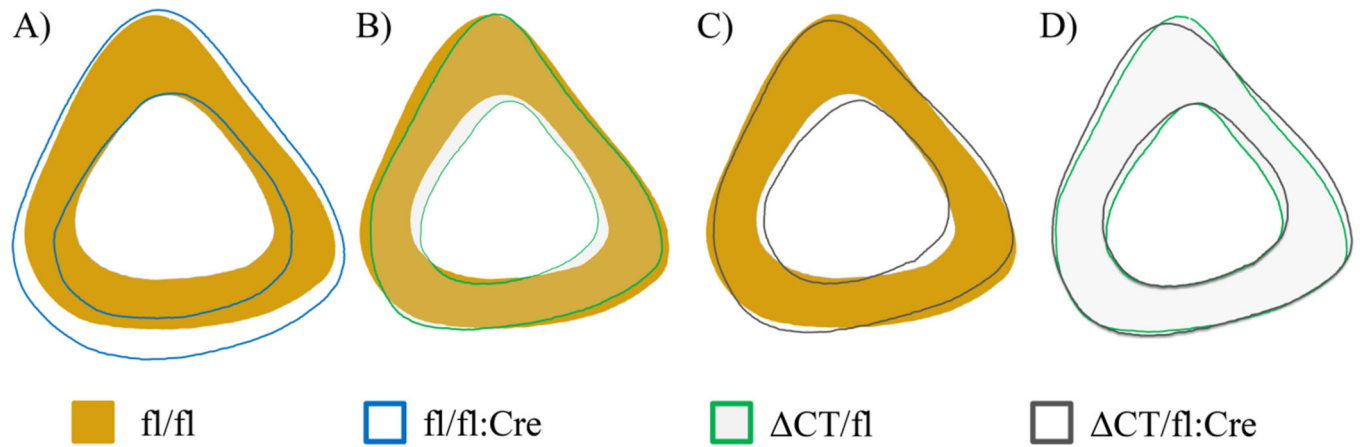
Figure 2.
Average profiles from standard cortical site in left tibiae. All profiles oriented with the anterior direction up and the medial direction to the right. A) Removing endogenous Cx43 from osteocytes results in cortical expansion in the posterior direction. B) Expressing the truncated form of Cx43 alongside endogenous Cx43 results in a thicker cortical shell due to an endocortical contraction. C) This endocortical contraction is maintained when truncated Cx43 is the only Cx43 expressed in osteocytes. D) The presence of the truncated form of Cx43 prevents the marked posterior periosteal expansion noted in panel A.

Figure 3.
Fracture toughness from mid-diaphysis of left tibiae. All three methods of calculating fracture toughness revealed a significant main effect of fl:Cre. The strongest effect was observed using the fracture instability method.

Table 1

Raman spectroscopy on medial surface of distal right tibiae

	fl/fl (n=9)	fl/fl:Cre (n=12)	CT/fl (n=7)	CT/fl:Cre (n=6)
Crystallinity [*]	0.0493 ± 0.0027	0.0515 ± 0.0029	0.0490 ± 0.0016	0.0508 ± 0.0025
CO_3^{2-}/PO_4^{3-}	0.380 ± 0.042	0.347 ± 0.026	0.375 ± 0.040	0.377 ± 0.044
$PO_4^{3-}/$Amide III	1.97 ± 0.31	2.02 ± 0.32	1.78 ± 0.27	1.98 ± 0.22

Data presented as mean ± SD.

[*] Main effect of fl:Cre.

Author Manuscript

Author Manuscript

Author Manuscript

Author Manuscript

Table 2

Reference point indentation on medial surface of distal right tibiae

	fl/fl (n=9)	fl/fl:Cre (n=12)	CT/fl (n=7)	CT/fl:Cre (n=6)
1st ID (μm)	36.9 ± 6.4	42.5 ± 7.6	36.8 ± 7.7	36.9 ± 9.8
1st ED (μJ)	33.9 ± 8.7	39.1 ± 9.4	33.6 ± 11.0	33.8 ± 13.1
1st US (N/μm)[†]	0.232 ± 0.020	0.206 ± 0.021	0.249 ± 0.025	0.240 ± 0.037
1st CID (μm)	4.74 ± 1.99	5.06 ± 1.32	4.58 ± 2.31	4.73 ± 2.17
IDI (μm)	8.76 ± 4.54	9.31 ± 3.20	8.01 ± 3.56	8.78 ± 4.33
TID (μm)	41.8 ± 8.9	47.7 ± 9.5	40.9 ± 8.7	41.8 ± 12.0
Total ED (μJ)	74.5 ± 14.6	83.8 ± 15.9	70.7 ± 15.4	79.8 ± 22.6
Avg CID (μm)	1.45 ± 0.44	1.62 ± 0.34	1.37 ± 0.45	1.53 ± 0.40
Avg ED (μJ)[*]	4.16 ± 0.68	4.63 ± 0.72	3.83 ± 0.60	4.80 ± 1.32
Avg US (N/μm)[†]	0.240 ± 0.020	0.215 ± 0.020	0.259 ± 0.024	0.250 ± 0.038

Data presented as mean ± SD.

[*] Main effect of fl:Cre

[†] Main effect of CT

Table 3

Trabecular analysis of proximal metaphysis of left tibiae

	fl/fl (n=8)	fl/fl:Cre (n=9)	CT/fl (n=7)	CT/fl:Cre (n=6)
BV/TV (%)	12.1 ± 3.4	14.1 ± 3.8	11.3 ± 4.1	12.3 ± 2.7
Tb.Th (μm) [†]	73.7 ± 4.5	73.8 ± 6.0	84.2 ± 4.1	82.3 ± 5.5
Tb.Sp (μm)	260 ± 47	238 ± 24	287 ± 49	268 ± 49
Tb.N (1/mm) [†]	1.64 ± 0.46	1.91 ± 0.48	1.34 ± 0.49	1.50 ± 0.33
SMI [†]	2.39 ± 0.23	2.26 ± 0.32	2.75 ± 0.38	2.67 ± 0.17
Conn.Dn (1/mm^3) [†]	72.4 ± 32.0	90.6 ± 34.0	48.9 ± 21.3	66.0 ± 32.7
BMD (g/cm^3 HA) [†]	0.134 ± 0.022	0.145 ± 0.028	0.115 ± 0.034	0.119 ± 0.029

Data presented as mean ± SD.

[†] Main effect of CT.

Table 4

Cortical analysis from diaphyseal standard site in left tibiae

	fl/fl (n=8)	fl/fl:Cre (n=9)	CT/fl (n=7)	CT/fl:Cre (n=6)
B.Ar (mm^2) [*] [†]	1.160 ± 0.078	1.414 ± 0.181	1.087 ± 0.106	1.135 ± 0.070
Ma.Ar (mm^2) [*] [†]	0.468 ± 0.044	0.695 ± 0.133	0.395 ± 0.03	0.433 ± 0.048
Ct.Ar (mm^2)	0.692 ± 0.041	0.718 ± 0.082	0.692 ± 0.077	0.701 ± 0.057
Ct.Wi (μm) [†]	220 ± 8	205 ± 22	232 ± 16	228 ± 18
Ps.Pm (mm) [#]	4.79 ± 0.18	5.23 ± 0.35[a]	4.70 ± 0.23	4.75 ± 0.14
Ec.Pm (mm) [*] [†]	3.08 ± 0.18	3.74 ± 0.42	2.89 ± 0.11	2.97 ± 0.14
I_{max} (mm^4) [#]	0.1084 ± 0.0159	0.1440 ± 0.0338[a]	0.0972 ± 0.0221	0.1015 ± 0.0127
I_{min} (mm^4) [*] [†]	0.0828 ± 0.0105	0.1067 ± 0.0227	0.0783 ± 0.0160	0.0832 ± 0.0105
TMD (g/cm^3 HA) [#]	1.192 ± 0.018	1.155 ± 0.037[a]	1.207 ± 0.024	1.217 ± 0.019

Data presented as mean ± SD.

[*] Main effect of fl:Cre.

[†] Main effect of CT.

[#] Interaction between main effects.

[a] Different from all other groups (determined by post hoc Tukey test if interaction present).